

# The effect of dopant concentration on properties of transparent conducting Al-doped ZnO thin films for efficient $\text{Cu}_2\text{ZnSnS}_4$ thin-film solar cells prepared by electrodeposition method

E. M. Mkawi · K. Ibrahim · M. K. M. Ali ·  
M. A. Farrukh · A. S. Mohamed

Received: 12 December 2014 / Accepted: 7 January 2015 / Published online: 22 January 2015  
© The Author(s) 2015. This article is published with open access at Springerlink.com

**Abstract** Al-doped ZnO (AZO) thin films were potentiostatically deposited on indium tin oxide substrates. The influence of the doping level of the ZnO:Al films was investigated. The results of the X-ray diffraction and scanning electron microscopy analysis revealed that the structural properties of the AZO films were found polycrystalline with a hexagonal wurtzite-type structure along the (002) plane. The grain size of the AZO films was observed as approximately 3  $\mu\text{m}$  in the film doping with 4 mol% ZnO:Al concentration. The thin films also exhibited an optical transmittance as high as 90 % in the wavelength range of 100–1,000 nm. The optical band gap increased from 3.33 to 3.45 eV. Based on the Hall studies, the lowest resistivity ( $4.78 \times 10^{-3} \Omega \text{ cm}$ ) was observed in the film doping with 3 mol% ZnO:Al concentration. The sheet resistant, carrier concentration and Hall mobility values were found as 10.78  $\Omega/\text{square}$ ,  $9.03 \times 10^{18} \text{ cm}^{-3}$  and 22.01  $\text{cm}^2/\text{v s}$ , respectively, which showed improvements in the properties of AZO thin films. The ZnO:Al thin films were used as a buffer layer in thin-film solar cells with the structure of soda-lime glass/Mo/ $\text{Cu}_2\text{ZnSnS}_4$ /ZnS/ZnO/Al grid. The best solar cell efficiency was 2.3 % with  $V_{\text{OC}}$  of 0.430 V,  $J_{\text{SC}}$  of 8.24  $\text{mA cm}^{-2}$  and FF of 68.1 %.

**Keywords** Electrochemical deposition · Aluminum-doped ZnO (ZnO:Al) films · Thin film · Electrical and optical properties

## Introduction

Transparent conductive oxides (TCOs) have several applications and used in solar cells and solar thermal applications due to their wide band gap (Jäger et al. 1998; Qiao et al. 2006). The widely explored transparent oxide semiconductors are a combination of  $\text{In}_2\text{O}_3$  and  $\text{SnO}_2$  such as indium tin oxide (ITO). However, the main constituents of ITO are rare, expensive and toxic. Zinc oxide (ZnO) is one alternative to ITO for fabrication of thin films for solar cell applications due to an inexpensive and non-toxic abundant material with suitable chemical and thermal properties. This is an n-type semiconductor having a hexagonal wurtzite structure with a wide band gap of 3.27 eV at room temperature (Kim et al. 2000) which perfectly matches the requirement of TCOs used as a window in solar cell application.

The resistivity of ZnO is usually up to  $10^4 \Omega \text{ cm}$ . However, the resistivity must be as low as possible to keep the required film thickness smaller for better current transport. Doping of different metals on ZnO helps to reduce the resistivity up to  $10^{-4} \Omega \text{ cm}$ . Several studies on ZnO doped with metals ( $\text{Al}^{+3}$ ,  $\text{In}^{+3}$ ,  $\text{Ga}^{+3}$ , etc.) have been conducted (Lee and Park 2004). Aluminum is commonly used as dopants for ZnO by replacing  $\text{Zn}^{+2}$  ions with  $\text{Al}^{+3}$  and showed photoluminescence in the ultraviolet (UV) and visible spectral range because of its optical properties and excitonic emission at room temperature (Wong and Season 1999). Aluminum-doped zinc oxide (ZnO:Al) has attracted

E. M. Mkawi (✉) · K. Ibrahim · M. K. M. Ali  
Nano-Optoelectronics Research and Technology Laboratory,  
School of Physics, Universiti Sains Malaysia, 11800 Penang,  
Malaysia  
e-mail: moizmerghnim@yahoo.com

M. A. Farrukh  
Department of Chemistry, GC University Lahore,  
Lahore 54000, Pakistan

A. S. Mohamed  
School of Chemical Sciences, Universiti Sains Malaysia,  
11800 Penang, Malaysia

much attention because of its low cost, good optical and electronic properties, heat stability, non-toxicity and high transparency in the near-infrared (IR) and invisible regions (90 %) (Ellmer et al. 1994). Several reports suggest that the obtainable resistivity in transparent conductive doped ZnO thin film depend on the crystallizations of the layer prepared on low-temperature substrates, dopant concentration and deposition technique (Minami et al. 1988, 1992; Hartnagel et al. 1995). It has been proven that the properties of aluminum-doped ZnO (AZO) thin films can be clearly improved by better deposition conditions and doping technique (Lee and Park 2003). Several methods have been adopted to prepare ZnO:Al films, such as chemical vapor deposition (Söderström et al. 2008), sputtering deposition (Tsai et al. 2006), spray pyrolysis (Zhao et al. 2005) and sol–gel method (Lee et al. 2011). The electrochemical deposition of ZnO:Al is the most promising deposition technique for low cost and large-area applications, which provides high-quality films with relatively high deposition rate at suitable substrate temperatures.

In this paper, ZnO:Al transparent conducting thin films were fabricated on ITO substrates and deposited via electrochemical deposition. The polyquaternium-2quaternized poly[bis(2-chloroethyl) ether-alt-1,3-bis[3-(dimethylamino) propyl]-urea] solvent was used to improvise the preferred orientation, electrical and optical properties of ZnO films, whereas monoethanolamine was used to increase the conductivity of the film and avoid colloids from aggregating. The influence of various Al concentrations between 1 and 4 mol% on the morphology and the electrical and optical properties of the deposited ZnO:Al films were investigated.

## Experimental

An ITO conducting glass substrate was deposited using an RF system at an argon flow rate of 20 cm<sup>3</sup>/min and working pressure of  $9 \times 10^{-3}$  mbar with a power of 150 W. ITO conductor has a typical sheet resistance of 35  $\Omega$ /square and thickness of about 500 nm. We selected ITO as a conductive layer due to electrical conductivity and optical transparency. Before that, the soda lime glass substrate was cleaned ultrasonically using acetone, isopropanol and absolute ethanol for 20 min. Copper wire ( $\sim 0.06$  mm in diameter) was first laid over the exposed ITO substrate in square shape, then covered with copper wire using polyimide heat-resistant/high-temperature adhesive tape. The active area of the substrates exposed to the electrolyte was 2.0 cm  $\times$  2.0 cm. This process will lead to facilitate good electrical contact. Electrochemical measurement was performed using a potentiostat/

galvanostat (E-corder 401 Potentiostat, Australia). The prepared ITO was used as working electrode, and an Ag/AgCl electrode in 3 M KCl was used as a reference electrode. A Pt mech was used as a counter electrode. The potential applied to the working electrode was changed from 0 to  $-0.9$  Vvs. NHE [with pulse time 600 ms and off-time (0 V) 600 ms] for 40 min to apply all the suitable voltages using to deposit aluminum and zinc.

All chemicals used were of reagent grade. An aqueous solution containing 0.4 M zinc nitrate [Zn(NO<sub>3</sub>)<sub>2</sub>·6H<sub>2</sub>O], Al(NO<sub>3</sub>)<sub>3</sub>·9H<sub>2</sub>O, 0.2 wt% polyquaternium-2quaternized poly[bis(2-chloroethyl) ether-alt-1,3-bis[3-(dimethylamino) propyl]-urea] solvent and monoethanolamine (MEA) was prepared in distilled water. Aqueous solutions are mixed together and made up to 60 mL with deionized water. The electrochemical cell glass put in water bath at 80 °C. The pH of the solution was 5. The distance between the platinum electrode and the substrate was 2 cm. Magnetic stirrer was used to make the solution homogeneous and improve the uniformity of the AZO film (100 rotations per min). After electrochemical deposition, the substrates were cleaned with deionized water at 100 °C to remove the salt residue source from the electrolyte solution. The thickness of the Al-doped ZnO films was controlled between 300 and 400 nm depending on deposition time, then the samples were annealed at 300 °C for 4 h in the air.

Solar cells were fabricated by chemical bath deposition of a CdS buffer layer (70 nm thick) on an as-deposited Cu<sub>2</sub>ZnSnS<sub>4</sub> (CZTS) thin-film absorber layer [fabricated on Mo-coated soda-lime glass as described in our previous work (Mkawi 2014)], followed by the deposition of 60-nm-thick i-ZnO and 500-nm-thick aluminum-doped zinc oxide layers using electrochemical deposition. The cells were completed by thermal evaporation of Al contacts, resulting in a cell structure of soda-lime glass/Mo/CZTS/CdS/i-ZnO/AZO/Al grid. The active area of each cell was 0.44 cm<sup>2</sup>.

The crystal structure and crystallinity of the prepared AZO nanostructures were characterized by X-ray diffraction (XRD) with CuK $\alpha$  radiation ( $k = 0.154056$  nm) (PANalyticalX'pert PRO MRD PW3040, The Netherlands). The morphology of the samples was analyzed using scanning electron microscopy (SEM) (JSM-6460, LV, Japan). The Hall mobility and carrier concentration were determined using four-point probe Hall effect measurements at room temperature (Accent/HL 5500 PC, UK). The band gap and energy spectral transmittance and reflectance of the AZO thin films at wavelengths 100–1,000 nm were measured using an HMZ-UV BROP-1800 ultraviolet–visible–near-infrared spectrophotometer (Japan).

## Results and discussion

### Morphological and structural properties

The surface morphology of the AZO layers deposited on the ITO substrate using the electrochemical deposition method as a function of various Al concentrations is shown in Fig. 1.

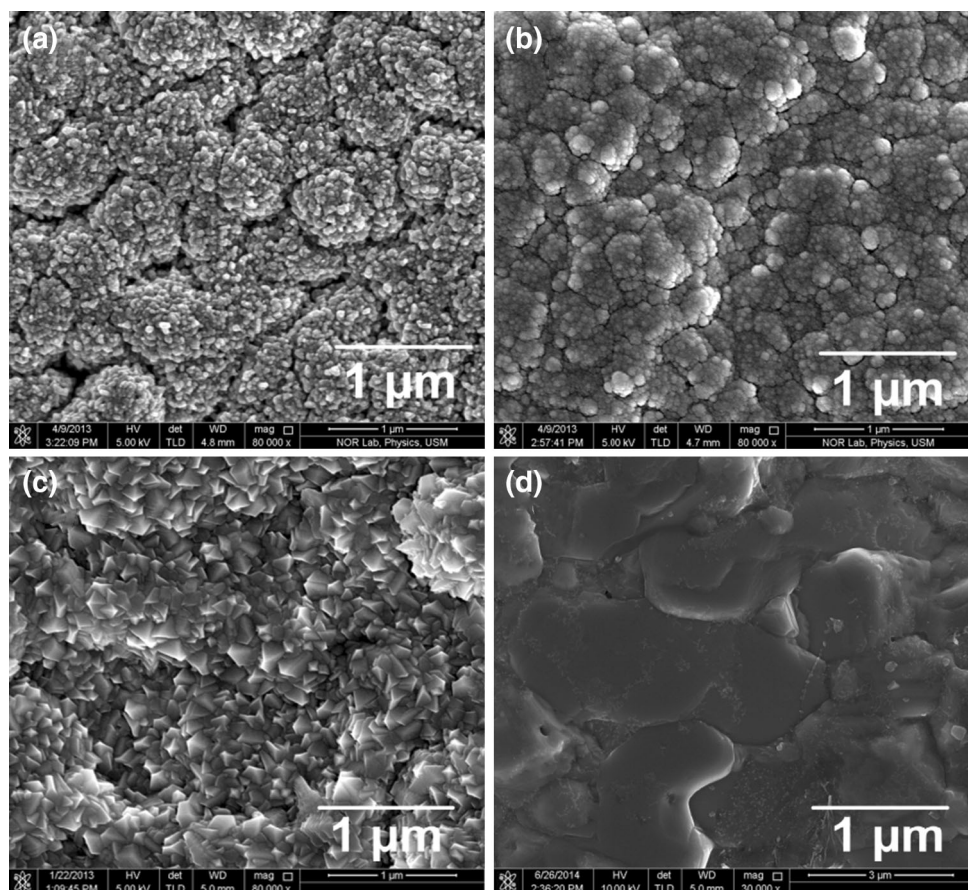
Figure 1a shows that microrods formed on ITO when solution prepared with Al concentration of 1 mol%. It is clear that the layer exhibited the poor crystalline quality of the films, and the surface is high roughness. Figure 1b shows that when Al concentration was increased to 2 mol%, few nanorods were formed which might be due to agglomerations of small crystallites that seem to be present in certain regions on the film surface. Figure 1c shows the surface changes in the film, wherein the sample formed clusters with large particle size at high  $\text{Al}^{+3}$  molar content when Al concentration was increased to 3 mol%. Furthermore, the film became denser and the change in particle size was due to the formation of stress resulting from a high difference in ionic radius between aluminum (0.057 nm) and zinc (0.074 nm) (Nunes et al. 2002). Figure 1d shows that when Al concentration was further increased to

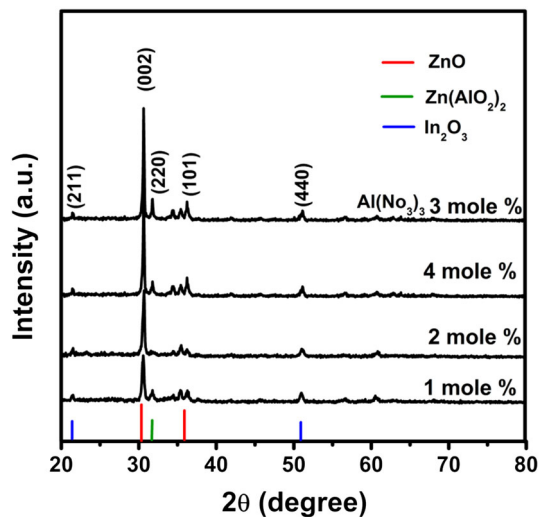
4 mol%, the particle size was observed bigger and well-formed grains ( $\sim 3 \mu\text{m}$ ) than Al concentration of 3 mol% were formed. The grains were interconnected, uniform and compact.

Figure 2 shows the XRD spectra in Bragg–Brentano geometry of the AZO samples at different concentrations of Al. The ITO layer appeared as  $\text{In}_2\text{O}_3$  in the XRD spectra at (211) and (440) (JCPDS 71-2194) (typically  $\text{In}_2\text{O}_3$  is 90 % of ITO) (Liang et al. 2001). The XRD pattern shows  $\text{Zn}(\text{AlO}_2)_2$  at (220) (JCPDS 002-1415) and  $\text{ZnO}$  at (101) and (002) (JCPDS 036-1451) (El Manouni et al. 2006). All samples exhibited an intensive hexagonal  $\text{ZnO}$  (002) plane, indicating a c-axis preferred orientation, which was significantly enhanced because of Al incorporation. The spectra showed very sharp diffraction peaks that indicate high crystallinity (Haller et al. 2011).

The peak (002) intensity increased with the increase in Al concentration. A maximum intensity was observed using 3 mol% of Al. However, the peaks decreased with the further increase in Al doping concentrations (more than 3 mol% of Al) indicating that an increase in Al doping concentration causes a deterioration in the film property. This result may be due to increased stress caused by the ion size differences between Al and Zn, as well as the

**Fig. 1** SEM images of doped AZO thin films with different aluminum contents **a** 1 mol%, **b** 2 mol%, **c** 4 mol%, and **d** 3 mol annealing at 300 °C for 4 h in the air





**Fig. 2** XRD patterns of ZAO films deposited on ITO contact with different aluminum concentrations from 1 to 4 mol% Al

formation, separation or segregation of aluminum in the grain boundaries at higher doping concentrations (Zhou et al. 2007). Furthermore, at higher doping concentrations, the nuclear charge of  $\text{Al}^{+3}$  arrests more oxygen than  $\text{Zn}^{+2}$  because  $\text{Al}^{+3}$  is larger than  $\text{Zn}^{+2}$ . Thus, the hexagonal structure and crystallinity of the thin films were decreased (Li et al. 2008).

The intensity of peak (101) was reduced with higher dopant concentrations. Hence, the higher dopant concentrations deteriorated the crystallinity of the thin film. A weak peak of Al was observed, indicating that Al replaced Zn in the lattice or Al transferred to the non-crystalline area in the grain boundary (Ayadi et al. 2008). At a concentration of 3 mol% Al, the quality of the AZO thin film improved based on the lowest value of the full width at half maximum (FWHM) of the (002) peak, which is a function of aluminum concentration. The FWHM of the (002) peak increased with the increase in doping concentration up to 3 mol% Al. The FWHM decreased at Al concentrations of 4 mol%, indicating that the number of the crystal planes depends on the microstress within a single crystallite or crystallite size (Berginski et al. 2007).

The grain size of the AZO nanoparticles was calculated from the FWHM of the (002) diffraction peak using the Scherrer formula as shown in Eq. 1.

$$D = \frac{0.9\lambda}{\beta \cos \theta} \quad (1)$$

where  $\lambda$  is the X-ray wavelength,  $\theta$  is the Bragg diffraction angle of the (002) peak and  $\beta$  is the full width at half maximum (FWHM) of the XRD peak. The average crystallite sizes along the c-axis were approximately 41 nm. The crystallite size was found to decrease with increasing Al content because of secondary phase growth, such as

**Table 1** Variation of crystallite size of AZO thin films on Al concentration

| Al concentration (mol%) | Crystallite size (nm) |
|-------------------------|-----------------------|
| (a) 1                   | 43.8                  |
| (b) 2                   | 43.3                  |
| (c) 3                   | 44.5                  |
| (d) 4                   | 39.6                  |

$\text{Al}_2\text{O}_3$ , which hinders the motion of the grain boundaries (Table 1). Good crystallized polycrystalline films with large grains have strong diffraction peaks and a narrow FWHM. With the increase in Al dopant, the (002) peak intensity rapidly increased and the FWHM decreased (Wan et al. 2010).

The XRD patterns were used to calculate the lattice constants,  $a = 3.2495 \text{ \AA}$  and  $c = 5.2069 \text{ \AA}$ . Based on the XRD patterns, the growth of  $\text{Zn}(\text{AlO}_2)_2$  indicates that Al can melt in ZnO crystal lattices uniformly. When the adsorbed Al was saturated, the structural phase changed because of the diffused Al in the ZnO lattice. This result was confirmed by the EDX results, which showed similar element contents for Zn and Al at several areas on the sample surface. The diffraction angle (variations in positions) of the (002) peak intensity was affected by the changes in Al concentrations, which may be due to some residual compressive stress inside the film, as reported by Kuroyanagi (1989).

### Optical properties

Figure 3 shows the transmission spectra of the AZO samples in the wavelength range of 100–1,000 nm using various Al doping concentrations. The average percentage transmittance in most of the visible region of the film ranged from 70 to 90 %. With a sharp fundamental absorption edge, a blue shift in the region of higher photon energy was observed with an increase in Al concentration. The visible transmission of these samples slightly increased when the Al concentration increased. This result may be due to the reduction of the voids in the sample and the improvement of the homogeneous structure with uniformly distributed particles, thereby increasing the optical scattering. The increased optical transmittance is related to the crystallinity of the film. The XRD results showed an increase in the intensity of the (002) peak with increasing Al concentration (Kim and Gilmore 2000).

With increasing  $\text{Al}^{+3}$  molar content, the absorption edge gradually shifted to a low-energy region, and the UV absorption and visible light transparency were significantly decreased up to 80 %. The slight shift in the absorption edge of the AZO caused the high carrier concentration

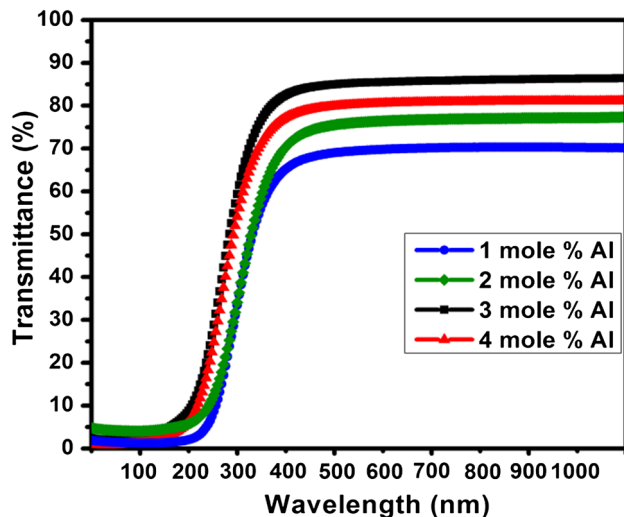


**Fig. 3** UV–vis transmittance spectra in the wavelength range 300–900 nm with different Al concentration annealing at 300 °C for 4 h in air

(Singh et al. 2004). In the IR region, the absorption of the film increased with the increase in Al concentration. Kim suggests that the increase in absorption may be due to Al doping (Kuroyangi 1989).

Figure 4 shows the optical energy gaps for the different ZnO:Al thin films deposited with different Al (NO<sub>3</sub>)<sub>3</sub>·9H<sub>2</sub>O concentrations. The absorption coefficient ( $\alpha$ ) was calculated from the optical transmission data to calculate the band gap. The optical band gap  $E_g$  can be calculated using the equation by Bardeen as shown in Eq. 2 (Tauc et al. 1966).

$$\alpha h\nu = A(h\nu - E_g)^n \quad (2)$$

where  $A$  is a constant, and  $n = 1/2$  or  $3/2$  for direct allowable transmission,  $h\nu$  the photon energy,  $\alpha$  is the absorption coefficient. Figure 4 shows the plot between  $(\alpha h\nu)^{1/2}$  and  $h\nu$  for the AZO samples at varying Al concentrations. Based on the location of the absorption edge, the optical energy gaps appeared in the range from 3.37 to 3.52 eV for the AZO films. The energy gap  $E_g$  initially increased when the Al concentration was increased up to 3 mol%, but the energy gap decreased when the Al doping was more than 3 mol%. This result agrees with previous reports (Suchea et al. 2007; Baik and Jang 1997).

The shift of the optical band gap to 3.55 eV can be explained by the Burstein–Moss effect as given in Eq. 3:

$$E_g = E_{g0} + \Delta E_g^{B-M} \quad (3)$$

where  $E_{g0}$  is the substantial energy gap and  $\Delta E_g^{B-M}$  is the Burstein–Moss effect (B–M) shift. The degree of freedom of the B–M shift is restricted and is directly proportional to the carrier concentration. The Burstein–Moss effect occurred during the Al doping of ZnO because the aluminum atoms replaced Zn in the ZnO lattice. The aluminum atoms worked singly as ionized donors, granting one extra electron. This electron occupied the bottom of the conduction band. Thus, the number of electrons increased as the doping concentration was increased, which widened the energy gap (Kim et al. 1999). Furthermore, at Al concentrations higher than 3 mol%, the resistivity increases because of the carrier concentration rather than the decrease in carrier mobility (Cebulla et al. 1998).

Photoluminescence (PL) was used to study the possible effects of Al doping and to check the optical quality of the samples. The shape of the PL spectra for all samples was almost identical using different Al concentrations for fabricating AZO with various surface roughness as shown in Fig. 5. The sharpest PL intensity at 380 nm wavelength attributed to the 3 mol% Al concentration corresponds to the UV emission. The increased intensity of UV emission was dependent on the crystal orientation and grain. As mentioned earlier, the peak (002) diffraction intensity and grain size increased as the doping concentration was increased. The calculated UV emission peaks also gradually increased when the Al doping was increased (Chen et al. 2008). In addition, the intensity of 380 nm was the sharpest among all of the peaks, which may be due to free exciton recombination and band-to-band transition. More specifically, the intensity of 377 nm may be due to band-to-band transition, the intensity of 380 nm may be due to free exciton recombination (Hsieh et al. 2007).

#### Electrical properties

The defects in hydrogen interstitial and oxygen vacancy and the addition of the Al<sup>+3</sup> dopant produced carriers in the films. Hydrogen interstitial variety of crystallographic defects in AZO case, Al and ZnO atoms which occupy a

**Table 2** Electrical property of AZO films deposited on glass substrate at 300 °C with various Al doping concentrations

| Al concentration (mol%) | Resistivity ( $\rho$ ) ( $\Omega$ cm) | Sheet resistant ( $R_s$ ) ( $\Omega$ /square) | Carrier concentration ( $N$ ) ( $\text{cm}^{-3}$ ) | Hall mobility $\mu_H$ ( $\text{cm}^2/\text{v s}$ ) |
|-------------------------|---------------------------------------|---|--|--|
| (a) 1                   | $7.82 \times 10^{-3}$                 | 13.78   | $6.78 \times 10^{18}$                              | 26.56  |
| (b) 2                   | $5.56 \times 10^{-3}$                 | 12.89   | $7.89 \times 10^{18}$                              | 23.67  |
| (c) 3                   | $4.78 \times 10^{-3}$                 | 10.78   | $9.03 \times 10^{18}$                              | 22.01  |
| (d) 4                   | $5.67 \times 10^{-3}$                 | 12.02   | $8.22 \times 10^{18}$                              | 20.69  |

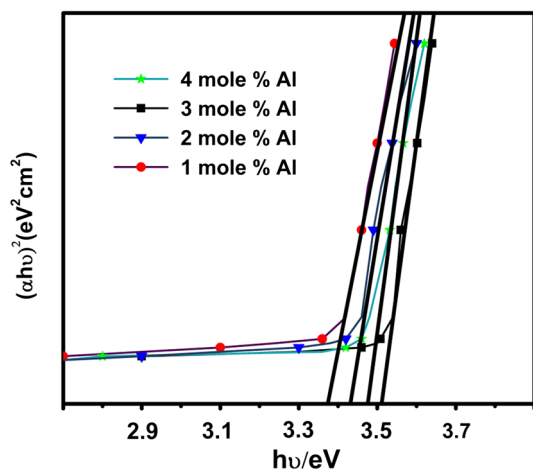


**Fig. 4** Plots of  $(\alpha hv)^2$  versus photon energy  $hv$  of ZnO:Al thin films with various Al concentrations

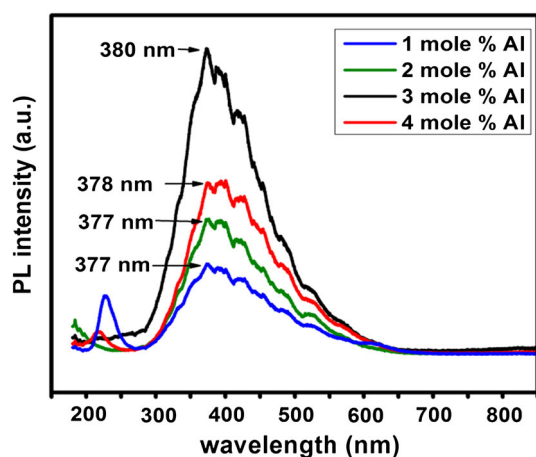


**Fig. 5** PL spectra of AZO thin film with a different Al concentration annealed at 300 °C for 4 h in the air

site in the crystal structure at which there is usually not an atom, or two or more atoms sharing one or more lattice sites such that the number of atoms is larger than the number of lattice sites. Oxygen vacancy is a type of point defect in a crystal sometimes referred to as crystalline defects. A defect in which an atom is missing from one of the lattice sites is known as a ‘vacancy’ defect. It is also known as a Schottky defect (Forsblom and Grimvall 2005). The electrical conductivity of the AZO films depended on the oxygen vacancies and the contribution from the Zn–Al interstitial atoms. The decrease in oxygen vacancies reduced the carrier concentration, thereby increasing the resistivity. The resistivity  $\rho$  of the AZO films decreased from  $7.82 \times 10^{-3}$  to  $4.78 \times 10^{-3} \Omega \text{ cm}$  as the Al concentration was increased from 1 to 3 mol% (Table 2). A slight increase in the resistivity ( $5.67 \times 10^{-3} \Omega \text{ cm}$ ) was observed when the Al concentration was higher than

3 mol%. This decrease in resistivity  $\rho$  can be attributed to the increase in the grain size of the AZO film. Thus, the conductivity was increased because of the reduction in the grain-boundary scattering. The increase in the free carrier concentration  $N$  cause to the decrease in resistivity  $\rho$ , carrier concentration  $N$  fabricated from the donor  $\text{Al}^{+3}$  ions incorporated as substitutions ions in  $\text{Zn}^{+2}$  ions as shown in Fig. 6. The conductivity increased due to the reduction in the number of oxygen vacancies in the AZO lattice (Kim et al. 2000). This increase in the carrier concentration also led to a decrease in the optical transmittance because of the increase in the free carrier absorption. The carrier concentration  $N$  decreased when Al concentrations were higher than 3 mol%, which may be due to the defects brought by the increase in Al dopant. Moreover, the Al atoms do not contribute free electrons. Meanwhile, the refractive index was inversely related to the carrier concentration  $N$ . Some reports suggested that when Al ions are incorporated in ZnO, the generation of free carriers increases with the increase in dopant concentration. The sheet resistance  $R_s$  of the samples initially decreased with increasing Al concentration, but suddenly increased when the concentration reached 3 mol%. The Hall mobility  $\mu_H$  gradually decreased with increasing Al content, which may have resulted from the ionized impurity prose. However, the decreased mobility with increasing Al content did not affect the grain size because the scattering frequency was controlled by the ionized impurity scattering and not the grain-boundary scattering for thick films above 700 nm (Kim et al. 2011). At lower Al concentrations, the carrier concentration  $N$  decreased because of the incorporation of Al into the substitutional sites, formation of  $\text{Al}_2\text{O}_3$ , or subsequent segregation of Al in the grain boundaries (Murdoch et al. 2009). Non-conducting  $\text{Al}_2\text{O}_3$  clusters grew due to the excess Al doped in the thin film, which produced defects and acted as carrier traps rather than electron donors. The optical band gap abruptly increased, resulting in poor

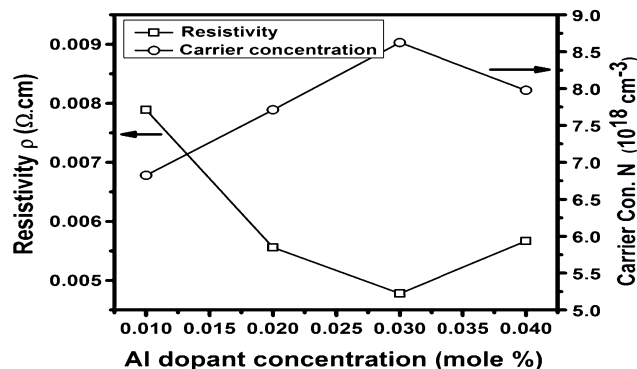


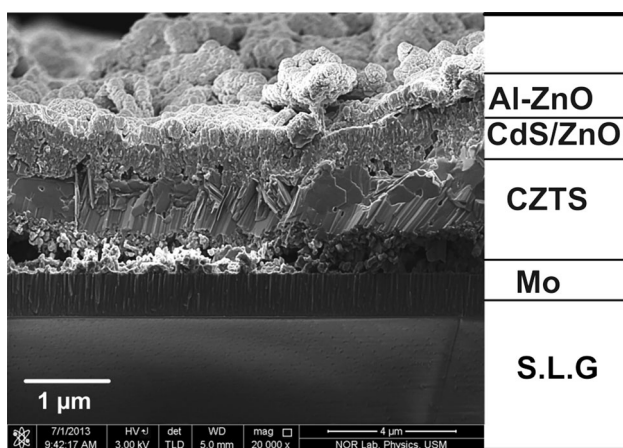
**Fig. 6** Resistivity ( $\rho$ ) of Al-doped ZnO on ITO with different aluminum concentrations

electrical conductivity. This increase in Al dopants also affected the mobility and decreased the crystal grain size. The larger grain size and decreased grain-boundary effect resulting from the increased carrier mobility increased the conductivity at a shorter range.

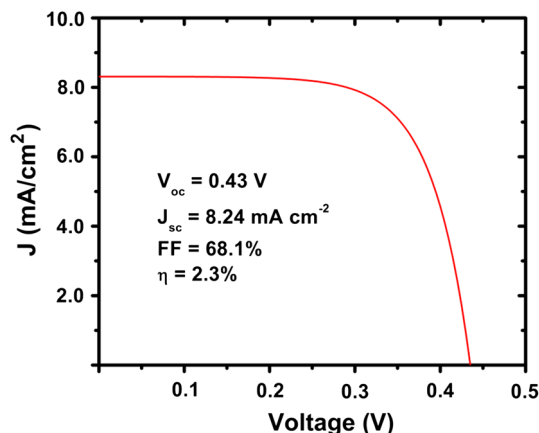
An optimal annealing temperature is necessary to improve electrical properties. With increasing annealing temperature, the crystal lattice deficiencies of the film in the grain boundaries decreased, resulting in an increase in the mobility of the carriers. At temperatures lower than 400 °C, large amount of Al impurities were found at the interstitial sites, and a high density of electrical dopants were found in the low areas of the AZO film. This effect caused by the electron mobility decreases the film defects (Ahn et al. 2011). In summary, Al<sup>3+</sup> works as an electrical dopant at low doping concentrations. However, the doped aluminum acts as an impurity at higher doping concentrations.

Figure 7 shows an FESEM cross section of the CZTS solar cells film using the film doping with 3 mol% ZnO:Al concentration as window layer, showing fewer voids and defects than the other films (not including) as well as a larger grain size. The cross-sectional micrograph shows a compact film with polyhedral-shaped grains.

Figure 8 shows the current density–voltage ( $J$ – $V$ ) characteristics of the CZTS solar cells under light irradiation, where  $J_{SC}$  is the short-circuit current density, FF is the fill factor and  $\eta$  is the conversion efficiency. CZTS solar cell fabricated using film doping with 3 mol% ZnO:Al concentration as window layer showed the highest efficiency of 2.3 % with  $V_{OC}$  of 0.430 V,  $J_{SC}$  of 8.24 mA cm<sup>-2</sup> and FF of 68.1 %. The improved device performance is caused by the high  $J_{SC}$  and  $V_{OC}$  of this device. Its high  $J_{SC}$  is attributed to its relatively large grains.



**Fig. 7** FE-SEM image of the broken cross section of a CZTS solar cell



**Fig. 8** Current–voltage characteristics of the best CZTS solar cell under illumination

## Conclusion

Al-doped ZnO thin films were successfully synthesized via electrochemical deposition on ITO substrates with various Al concentrations at a solution temperature of 80 °C. The effects of aluminum concentration on the structural, morphological, electrical and optical characteristics of the AZO thin films were studied. The AZO thin films had a preferential c-axis orientation crystalline structure. The 3 mol% Al films exhibited a hexagonal wurzite structure with (002) preferred crystal orientation, as well as the best optical properties and electrical conductivity among all the samples. The main peak (002) slightly shifted in position with the increase in Al doping. The main role of the electron carrier concentration based on the Al content of the AZO films was also investigated. The lowest resistivity [ $4.78 \times 10^{-3} \rho$  ( $\Omega$  cm)] was obtained by the film with 3 mol% Al concentration. The transmissions were as high as 90 % in the wavelength range of 100–1,000 nm and depended on the dopant concentration. The Al-doped ZnO thin film showed high transmittance and crystallinity, as well as low resistivity, depending on the dopant concentration. The best cell fabricated with a ZnS thin film grown at 500 °C exhibited a conversion efficiency of 2.3 % with an open-circuit voltage of 0.430 V, short-circuit current density of 8.24 mA/cm<sup>2</sup> and fill factor of 68.1 %.

**Acknowledgments** This work was supported by the Nano-optoelectronics Research Laboratory, School of Physics: Universiti Sains Malaysia under Grant Number 203/PSF-6721001.

**Open Access** This article is distributed under the terms of the Creative Commons Attribution License which permits any use, distribution, and reproduction in any medium, provided the original author(s) and the source are credited.

## References

- Ahn CH, Kong BH, Kim H, Cho HK (2011) Improved electrical stability in the Al doped ZnO thin-film-transistors grown by atomic layer deposition. *J Electrochem Soc* 158:H170–H173
- Ayadi, Emir L, Djessas K, Alaya S (2008) The properties of aluminum-doped zinc oxide thin films prepared by rf-magnetron sputtering from nanopowder targets. *Mater Sci Eng C* 28:613–617
- Baik SJ, Jang JH, Lee CH, Cho WY, Lim KS (1997) Highly textured and conductive undoped ZnO film using hydrogen post-treatment. *Appl Phys Lett* 70:3516–3518
- Berginski M, Hüpkens J, Schulte M, Schöpe G, Stiebig H, Rech B (2007) The effect of front ZnO: Al surface texture and optical transparency on efficient light trapping in silicon thin-film solar cells. *J Appl Phys* 101:074903–079114
- Cebulla R, Wendt R, Ellmer K (1998) Al-doped zinc oxide films deposited by simultaneous rf and dc excitation of a magnetron plasma: relationships between plasma parameters and structural and electrical film properties. *J Appl Phys* 83:1087–1095
- Chen KJ, Fang TH, Hung FY, Ji LW, Chang SJ, Young SJ, Hsiao YJ (2008) The crystallization and physical properties of Al-doped ZnO nanoparticles. *Appl Surf Sci* 254:5791–5795
- El Manouni A, Manjón FJ, Mollar M, Marí B, Gómez R, López MC, Ramos-arrado JR (2006) Effect of aluminium doping on zinc oxide thin films grown by spray pyrolysis. *Superlattices Microstruct* 39:185–192
- Ellmer K, Kudella F, Mientus R, Schieck R, Fiechter S (1994) Influence of discharge parameters on the layer properties of reactive magnetron sputtered ZnO: Al films. *Thin Solid Films* 247:15–23
- Forsblom M, Grimvall G (2005) Homogeneous melting of superheated crystals: molecular dynamics simulations. *Phys Rev B* 72:054107
- Haller S, Rousset J, Renou G, Lincot D (2011) Electrodeposition of nanoporous ZnO on Al-doped ZnO leading to a highly organized structure for integration in dye sensitized solar cells. *EPJ Photovoltaics* 2:20401
- Hartnagel HL, Dawar AL, Jain AK, Jagadish C (1995) *Semiconducting transparent thin films*, 1st edn. IOP Publishing Ltd, Bristol, p 22
- Hsieh PT, Chen YC, Kao KS, Lee MS, Cheng CC (2007) The ultraviolet emission mechanism of ZnO thin film fabricated by sol–gel technology. *J Eur Ceram Soc* 27:3815–3818
- Jäger S, Szyszka B, Szczyrbowski J, Bräuer G (1998) Comparison of transparent conductive oxide thin films prepared by ac and dc reactive magnetron sputtering. *Surf Coat Technol* 98:304–314
- Kim H, Gilmore CM (2000) Transparent conducting aluminum-doped zinc oxide thin films for organic light-emitting devices. *Appl Phys Lett* 76:259–261
- Kim H, Gilmore CM, Pique A, Horwitz JS, Mattoussi H, Murata H, Kafafi ZH, Chrisey DB (1999) Electrical, optical, and structural properties of indium–tin–oxide thin films for organic light-emitting devices. *J Appl Phys* 86:6451–6461
- Kim H, Gilmore CM, Horwitz JS, Pike A, Murata H, Kushto GP, Schlaf R, Kafafi ZH, Chrisey DB (2000a) Transparent conducting aluminum-doped zinc oxide thin films for organic light-emitting devices. *Appl Phys Lett* 76:259–261
- Kim H, Pique A, Horwitz JS, Murata H, Kafafi ZH, Gilmore CM, Chrisey DB (2000b) Effect of aluminum doping on zinc oxide thin films grown by pulsed laser deposition for organic light-emitting devices. *Thin Solid Films* 377:798–802
- Kim WH, Maeng WJ, Kim MK, Kim H (2011) Low pressure chemical vapor deposition of aluminum-doped zinc oxide for transparent conducting electrodes. *J Electrochem Soc* 158:D495–D499
- Kuroyanagi A (1989) Crystallographic characteristics and electrical properties of Al-doped ZnO thin films prepared by ionized deposition. *J Appl Phys* 66:5492–5497
- Kuroyanagi A (1989) Crystallographic characteristics and electrical properties of Al-doped ZnO thin films prepared by ionized deposition. *Jpn J Appl Phys* 28:219–222
- Lee JH, Park BO (2003) Transparent conducting ZnO: Al, In and Sn thin films deposited by the sol–gel method. *Thin Solid Films* 426:94–99
- Lee JH, Park BO (2004) Characteristics of Al-doped ZnO thin films obtained by ultrasonic spray pyrolysis: effects of Al doping and an annealing treatment. *Mater Sci Eng B* 106:242–245
- Lee KE, Wang M, Kim EJ, Hahn SH (2011) Structural, electrical and optical properties of sol–gel AZO thin films. *Curr Appl Phys* 9:683–687
- Li LJ, Deng H, Dai LP, Chen JJ, Yuan QL, Li Y (2008) Properties of Al heavy-doped ZnO thin films by RF magnetron sputtering. *Mater Res Bull* 43:1456–1462
- Liang H, Meng G, Lei Y, Philipp F, Zhang L (2001) Catalytic growth of semiconducting In<sub>2</sub>O<sub>3</sub> nanofibers. *Adv Mater* 13:17
- Minami T, Nanto H, Sato H, Takata S (1988) Effect of applied external magnetic field on the relationship between the arrangement of the substrate and the resistivity of aluminium-doped ZnO thin films prepared by r.f. magnetron sputtering. *Thin Solid Films* 164:275–279
- Minami T, Sato H, Imamoto H, Takata S (1992) Substrate temperature dependence of transparent conducting Al-doped ZnO thin films prepared by magnetron sputtering. *Jpn J Appl Phys* 31:257
- Mkawi EM, Ibrahim K, Ali MKM, Farrukh MA, Mohamed AS (2014) Dependence of the properties of copper zinc tin sulfide thin films prepared by electrochemical deposition on sulfuration temperature. *J Mater Sci Mater Electron* 25:857–863
- Murdoch GB, Hinds S, Sargent EH, Tsang SW, Mordoukhovski L, Lu ZH (2009) Aluminum doped zinc oxide for organic photovoltaics. *Appl Phys Lett* 94:213301–213303
- Nunes P, Fortunato E, Tonello P, BrazFernandes F, Vilarinho P, Martins R (2002) Effect of different dopant elements on the properties of ZnO thin films. *Vacuum* 64:281–285
- Qiao Z, Agashe C, Mergel D (2006) Dielectric modeling of transmittance spectra of thin ZnO: Al films. *Thin Solid Films* 496:520–525
- Singh AV, Mehta RM, Yoshida A, Wakahara A (2004) Doping mechanism in aluminum doped zinc oxide films. *J Appl Phys* 95:3640–3643
- Söderström T, Haug FJ, Niquille X, Ballif C (2009) TCOs for nip thin film silicon solar cells. *Prog Photovoltaics Res Appl* 17:165–176
- Suchea M, Christoulakis S, Katsarakis N, Kitsopoulos T, Kiriakidis G (2007) Comparative study of zinc oxide and aluminum doped zinc oxide transparent thin films grown by direct current magnetron sputtering. *Thin Solid Films* 515:6562–6566
- Tauc J, Grigorovici R, Vancu A (1966) Optical properties and electronic structure of amorphous germanium. *Phys Status Solidi B* 15:627–637
- Tsai SY, Lu YM, Lu JJ, Hon MH (2006) Comparison with electrical and optical properties of zinc oxide films deposited on the glass and PET substrates. *Surf Coat Technol* 200:3241–3244
- Wan D, Huang F, Wang Y (2010) Highly surface-textured ZnO: Al films fabricated by controlling the nucleation and growth separately for solar cell applications. *Am Chem Soc* 2:2147–2152
- Wong EM, Season PC (1999) ZnO quantum particle thin films fabricated by electrophoretic deposition. *Appl Phys Lett* 74:2939–2941



Zhao JL, Li XM, Bian JM, Yu WD, Zhang CY (2005) Growth of nitrogen-doped p-type ZnO films by spray pyrolysis and their electrical and optical properties. *J Cryst Growth* 280:495–501

Zhou H, Yi D, Yu Z, Xiao L, Li J (2007) Growth of nitrogen-doped p-type ZnO films by spray pyrolysis and their electrical and optical properties. *Thin Solid Films* 515:6909–6914